Sustainable Marine Structures
https://journals.nasspublishing.com/index.php/sms

ARTICLE

A Fuzzy Legendre-Green Function Method for Hydro-Elastic Wave Attenuation in Flexible Porous Floating Breakwaters

Yogeesh Nijalingappa [1,2*] , ***Asokan Vasudevan*** [3] , ***Manchaiah Savithramma Sunitha*** [2], ***Suleiman Ibrahim Mohammad*** [1], ***Kanchugaranahalli Chandrappa Jagadeesha*** [2]

[1] *Research Fellow, INTI International University, Nilai 71800, Malaysia*

[2] *Department of Mathematics, Government First Grade College, Tumkur 572102, India*

[3] *Faculty of Business and Communications, INTI International University, Nilai 71800, Malaysia*

ABSTRACT

The present study forms a compact hydro-elastic benchmark of a flexible porous floating breakwater, with bounded parameter uncertainty. The floating member is represented as a discrete-semicontinuum Euler-Bernoulli beam in the frequency domain, and it interacts with an oscillatory-decay hydrodynamic kernel in the finite-depth approximation. A structural Green function is presented, transforming the governing boundary-value problem into the solution of a Fredholm integral equation of the second kind, which is solved by means of Legendre-Gauss-Lobatto collocation. The impact of uncertainty in flexural rigidity, structural mass, damping and depth ratio, porous dissipation and forcing amplitude is modeled by triangular fuzzy numbers; alpha-cut analysis using vertex evaluation with nesting correction propagates the uncertainty. The benchmark results show a sharp resonance region where the structural response and transmission loss become increasingly sensitive to parameter variation, while the admissible response band is narrow off-resonance. The derived formulation also provides a computationally lightweight framework for joint assessment of wave attenuation and structural demand. This study is mathematically and numerically transparent, computationally light, and easy to extend to many relevant situations. The results discussed in this study also showed that uncertainty is concentrated near the spatial region of maximum structural

*CORRESPONDING AUTHOR:
Yogeesh Nijalingappa, Research Fellow, INTI International University, Nilai 71800, Malaysia; Department of Mathematics, Government First Grade College, Tumkur 572101, India; Email: yogeesh.r@gmail.com

ARTICLE INFO
Received: 25 March 2026 | Revised: 6 April 2026 | Accepted: 16 April 2026 | Published: 14 May 2026
DOI: https://doi.org/10.36956/sms.v8i2.3215

CITATION
Nijalingappa, Y., Vasudevan, A., Sunitha, M.S., et al., 2026. A Fuzzy Legendre-Green Function Method for Hydro-Elastic Wave Attenuation in Flexible Porous Floating Breakwaters. Sustainable Marine Structures. 8(2):162–176. DOI: https://doi.org/10.36956/sms.v8i2.3215

response and that, for the chosen benchmark, porous dissipation and forcing level are the most influential inputs.
Keywords: Coastal Protection; Spectral Collocation; Nonlocal Hydrodynamic Kernel; Porous Damping; Transmission Loss; Marine Flexural Response; $\alpha - cut$ Propagation

1. Introduction

Flexible floating breakwaters have recently gained renewed attention, as coastal protection systems are needed to operate in deeper water, over soft seabeds, and under more stringent construction and sustainability constraints. In these environments, hydro-elastic interaction is no longer a higher-order correction: distributed flexibility, porous appendages and unknown material or hydrodynamic properties can move resonance and alter attenuation and structural demand. This work is motivated by that design gap and targets a reduced benchmark that is mathematically transparent but retains the central coupled mechanisms.

Floating breakwaters are a preferred option when it is difficult, or too expensive, to build a normal fixed breakwater. This is common in deeper water over weak seabeds or at sites where a lighter and more adaptable protection system is much preferred. In many experimental studies with more vibrant situations, the floating unit is treated as rigid in its state [1–4]. Once flexibility becomes an important aspect, the structural motion and the surrounding water cannot be separated in the given situation [5]. Wave loading bends the floating member, and that bending changes the pressure field acting on the selected structure [6–8].

As related to this study, recent studies have shown growing interest in hydro-elastic floating systems and the reviews by Amouzadrad et al. and Zhang and Schreier [2, 3] describe how flexible floating structures can experience strong coupled responses, especially near resonant conditions. Other studies have also shown that simplified rigid-body models are not always sufficient when the span is large or when distributed flexibility is relatively important [9, 10]. The concept of research on floating breakwaters follows the same trend that was discussed by Jia et al. [6] and he reported that flexible wave-dissipating elements can improve attenuation behavior, while Ren et al. and Pan et al. [4, 5] both examined hydro-elastic modeling strategies for flexible floating structures under wave loading.

Although deterministic hydro-elastic tools are now well developed, uncertainty propagation remains less mature. Yogeesh et al. and Rahmatov conducted sensitivity and uncertainty analysis for floating offshore structures and noted that structural parameters, connectors, mooring terms, and hydrodynamic descriptors can materially affect hydro-elastic predictions [11–13]. In early-stage design, however, a full probabilistic description is often not available. Rigidity, damping, porosity effect, and representative forcing amplitude may be bounded by engineering judgement or sparse test data, but not by a defensible probability distribution [14–17]. In that setting, fuzzy uncertainty is a useful alternative because it represents plausible bounds directly and transparently [18, 19]. Triangular fuzzy numbers and $\alpha - cuts$ are particularly attractive when the goal is to provide an engineering response band rather than a probabilistic risk measure.

The purpose of this paper is therefore to develop a fuzzy Legendre-Green function method for the hydro-elastic analysis of a flexible porous floating breakwater. The paper is designed as a theory-led benchmark study. It does not attempt to reproduce one specific field site. Instead, it develops a transparent dimensionless model that can later be calibrated for design use. The main contributions are: a nonlocal hydro-elastic beam model for a flexible porous floating breakwater; a Green-function reduction to a Fredholm integral equation of the second kind; a Legendre-Gauss-Lobatto collocation solver; a fuzzy alpha-cut formulation for uncertain rigidity, mass, damping, porosity effect, depth ratio, and forcing amplitude; deterministic and fuzzy benchmark results for structural and attenuation metrics; and a sensitivity analysis that identifies the dominant parameters in the present benchmark. Section 2 presents the physical model, Green-function reduction, collocation discretization, and fuzzy propagation strategy. Section 3 reports

deterministic, fuzzy, and sensitivity results. Section 4 discusses the physical implications, model validity, and present limitations. Section 5 summarizes the main conclusions.

A second challenge is computational. Hydro-elastic beam problems are often written as coupled differential or integro-differential equations. Direct discretization is possible, but repeated solution over many uncertainty realizations can become expensive, and the role of the structural boundary conditions is sometimes obscured by the discretization. Green functions provide a tidy solution as they automatically incorporate the structural boundary conditions directly in the kernel and cast the beam problem into one of integral equations. Once that reduction is made, spectral collocation on Legendre or Chebyshev points provides an accurate and economical numerical solver for smooth responses. Collocation ideas have also been used effectively in structural fuzzy uncertainty analysis [15–17].

The purpose of this paper is therefore to develop a fuzzy Legendre-Green function method for the hydro-elastic analysis of a flexible porous floating breakwater. The paper is designed as a theory-led benchmark study. It does not attempt to reproduce one specific field site. Instead, it develops a transparent dimensionless model that can later be calibrated for design use. The main contributions are: a nonlocal hydro-elastic beam model for a flexible porous floating breakwater; a Green-function reduction to a Fredholm integral equation of the second kind; a Legendre-Gauss-Lobatto collocation solver; a fuzzy $\alpha - cut$ formulation for uncertain rigidity, mass, damping, porosity effect, depth ratio, and forcing amplitude; deterministic and fuzzy benchmark results for structural and attenuation metrics; and a sensitivity analysis that identifies the dominant parameters in the present benchmark.

2. Materials and Methods

The simply supported condition is adopted here as a benchmark support model rather than as a universal representation of every moored breakwater. It regularizes the rigid-body singularity, provides a compact modal Green function, and isolates the flexural hydro-elastic mechanism that dominates. While resonances would be displaced by clamped, elastically restrained or mooring-controlled edges that might be present in practice, the current choice of support is suitable for a clear baseline study.

For instance, the local flow separation and the resultant pressure pattern in the near-field can be influenced by fluid motion in close vicinity to a submerged porous edge. The present reduced formulation does not resolve these edge-scale effects explicitly, but rather absorbs this information in the effective kernel and porous dissipation terms. This should be considered a baseline approximation instead of an actual replacement within the routine boundary-element or Navier-Stokes treatment.

2.1. Physical Configuration and Modeling Assumptions

The floating breakwater is an Euler-Bernoulli beam with nondimensional span 1, resting at the surface of a water depth ratio $\delta = h/L;\ x \in [0,1];\ W(x)$ is the complex vertical response amplitude in the frequency domain. A porous skirt or dissipative layer is attached below the beam, and its hydrodynamic effect is represented through an additional porous damping contribution and through the attenuation closure introduced later. The benchmark uses a simply supported structural idealization, and this choice is convenient because it removes rigid-body singularities and produces a compact Green-function representation while still preserving the principal flexural hydro-elastic mechanism.

The analysis is based on the following assumptions: small-amplitude motion, linear Euler-Bernoulli bending, incompressible and irrotational fluid motion within the reduced hydrodynamic model, harmonic regular-wave forcing, and bounded epistemic uncertainty described by fuzzy numbers (see **Figure 1**). These assumptions keep the model manageable and are in line with many reduced hydro-elastic beam formulations used in marine engineering [1–5, 15].

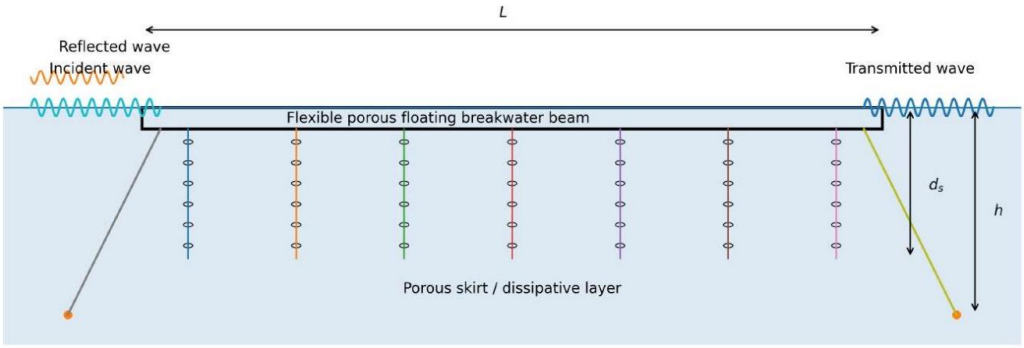

Figure 1. The geometry of a flexible porous floating breakwater beam.

The benchmark reflects a simply supported floating beam along with a porous dissipative appendage placed below the required free surface.

The below-mentioned principal dimensionless parameters are:

- β: normalized flexural rigidity,
- μ: normalized structural mass,
- γ_s: structural damping,
- δ: depth-to-length ratio,
- σ: porous dissipation coefficient,
- a: normalized forcing amplitude,
- Ω: nondimensional wave frequency.

2.2. Frequency-Domain Hydro-Elastic Equation

Assume harmonic motion in the form:

$$w(x,t) = \Re\left\{W(x)e^{-i\omega t}\right\}.$$

After the non-depersonalization, the response of the floating breakwater is expressed as:

$$\beta\frac{d^4W}{dx^4} - \Omega^2\mu W - i\Omega\gamma W + \int_0^1 K(x,\xi;\Omega,\delta)W(\xi)d\xi = F(x;\Omega),\ 0 < x < 1,$$

where the total damping is:

$$\gamma = \gamma_s + \gamma_p,\ \gamma_p = \frac{\sigma\Omega}{1+\delta\kappa}.$$

The simply supported boundary conditions are:

$$W(0) = W(1) = 0,\ W^{''}(0) = W^{''}(1) = 0.$$

Here, the benchmark forcing is selected as the first-mode-compatible load:

$$F(x;\Omega) = a\sin(\pi x)$$

This load is not intended to replace a full diffraction calculation as per the discussion of this study. It is chosen because it excites the dominant flexural mode cleanly and allows us to uncover how resonance, porous dissipation and, in addition, parameter uncertainty mutually influence[20–23].

2.3. Reduced Finite-Depth Hydrodynamic Kernel

The nonlocal fluid interaction is represented by a reduced finite-depth oscillatory-decay kernel:

$$K(x,\xi;\Omega,\delta) = \chi_h(\Omega,\delta)\exp(-\eta(\Omega,\delta)|x-\xi|)\cos(\kappa(\Omega,\delta)(x-\xi)).$$

The wave number κ is defined through the finite-depth dispersion relation.

Then we present the reduced kernel as an approximation for benchmarking. It retains three properties necessary for the current analysis: nonlocal coupling, finite-distance decay, and oscillation of the wave phase. A complete potential-flow or boundary-element solution would give higher fidelity across all frequencies, but the current kernel is designed for reduced-model benchmarking and repeated uncertainty propagation, not detailed site-specific calibration.

$$\Omega^2 = \kappa\tanh(\delta\kappa).$$

The kernel amplitude and decay rate are represented as:

$$\chi_h(\Omega,\delta) = \frac{\chi_0\Omega^2}{1+\delta\kappa},\ \eta(\Omega,\delta) = 0.45 + 0.25\kappa.$$

Here $\chi_0 = 0.15$ in baseline benchmark and the reduced kernel is designed to be compact. Notice, however, that it retains three characteristics that are very

much relevant to the current hydro-elastic paradigm and a through nonlocality and decay with structural distance as well as oscillatory behavior associated with the wave number [24, 25].

2.4. Green-Function Reduction

Define the structural operator:

$$\mathcal{L}_\Omega W = \beta W^{(4)} - \Omega^2 \mu W - i\Omega\gamma W.$$

Let $G(x, \xi; \Omega)$ be the Green function satisfying the equation with the same simply supported boundary conditions in x.

$$\mathcal{L}_\Omega G(x, \xi; \Omega) = \delta(x - \xi).$$

No singular quadrature treatment is required in the present benchmark because the structural Green function is regular for the chosen simply supported beam and the reduced hydrodynamic kernel is smooth over the finite interval. The derivation relies on standard regularity assumptions for linear beam response with smooth forcing and bounded kernel coefficients, so the resulting Fredholm equation is well posed in the present numerical setting.

For the simply supported beam, the Green function has the modal series representation as given below:

$$G(x, \xi; \Omega) = \sum_{n=1}^{\infty} \frac{2\sin(n\pi x)\sin(n\pi\xi)}{\beta(n\pi)^4 - \Omega^2\mu - i\Omega\gamma}.$$

Using this Green function and the hydro-elastic problem is transformed into the Fredholm integral equation of the second kind that is given by:

$$W(x) = \int_0^1 G(x, \xi; \Omega) \left[F(\xi; \Omega) - \int_0^1 K(\xi, s; \Omega, \delta) W(s)\, ds\right] d\xi$$

The Green-function step is central to the method and it places the structural boundary conditions inside the kernel itself and changes the numerical problem from repeated differentiation to quadrature and linear algebra [26].

A useful one-mode approximation follows by writing:

$$W(x; \Omega) \approx A_1(\Omega)\sin(\pi x).$$

Then:

Legendre-Gauss-Lobatto collocation, which spaces nodes at both interval endpoints, is employed for its compliance with the finite-span geometry, and stable high-order interpolation of smooth response fields. This is particularly useful in the current integral-equation context, as moderate collocation orders are already sufficient to accurately approximate the benchmark solution [27, 28].

$$A_1(\Omega) = \frac{a}{D_1(\Omega)},$$

where the effective resonance denominator is given by:

$$D_1(\Omega) = \beta\pi^4 - \Omega^2\mu - i\Omega\gamma + \Lambda_1(\Omega, \delta),$$

and the first-mode hydrodynamic correction is expressed as:

$$\Lambda_1(\Omega, \delta) = 4\int_0^1 \int_0^1 K(x, \xi; \Omega, \delta)\sin(\pi x)\sin(\pi\xi) d\xi dx.$$

However, this approximation is not the main solver utilized in this work, yet it is useful when analyzing resonance and as well sensitivity trends.

2.5. Legendre-Gauss-Lobatto Collocation

Let $\zeta_j \in [-1, 1]$ be the Legendre-Gauss-Lobatto points defined by the roots of:

$$\left(1 - \zeta^2\right) L_N^{'}(\zeta) = 0,$$

where $L_N^{'}(\zeta)$ is the Legendre polynomial of degree N; then after mapping to the unit interval,

$$(x_j = \frac{1 + \zeta_j}{2},\ j = 0, 1, \ldots, N.$$

The quadrature weights on $[0, 1]$ are:

$$w_j = \frac{1}{N(N + 1)\left[L_N(\zeta_j)\right]^2}.$$

The approximate response is expressed in the equation as:

$$W_N(x) = \sum_{j=0}^{N} W_j \boldsymbol{\ell}_j(x),$$

where $l_j(x)$ is the Lagrange interpolation function corresponding to the Legendre-Gauss-Lobatto points. Substituting this interpolant into the integral equation being represented and enforcing the result at collocation nodes yields, which is given by

$$W_i = \sum_{j=0}^{N} G(x_i, x_j; \Omega) w_j \left[F(x_j; \Omega) - \sum_{k=0}^{N} K(x_j, x_k; \Omega, \delta) w_k W_k\right].$$

In matrix form,

$$(I + G_w K_w)\, W = G_w F,$$

with:

$$(G_w)_{ij} = G\,(x_i, x_j; \Omega)\, w_j,\ (K_w)_{jk} = K\,(x_j, x_k; \Omega, \delta)\, w_k.$$

Solve the matrix system for each frequency and for each parameter realization. For this current benchmark, the response is smooth enough that fairly moderate collocation orders already yield stable and correct results [29].

2.6. Fuzzy Uncertainty Model

The uncertain parameter vector is defined as:

$$\widetilde{p} = \left(\widetilde{\beta}, \widetilde{\mu}, \widetilde{\gamma}_s, \widetilde{\delta}, \widetilde{\sigma}, \widetilde{a}\right).$$

Each uncertain quantity is represented by a triangular fuzzy number:

$$\widetilde{p} = (p_1, p_2, p_3)\,,\ p_1 \le p_2 \le p_3,$$

with $\alpha - cut$

$$[\widetilde{p}]^{\alpha} = [p_1 + \alpha\,(p_2 - p_1)\,, p_3 - \alpha\,(p_3 - p_2)]\,,\ 0 \le \alpha \le 1.$$

The reason we use a triangular membership function is that only bounded three-point engineering estimates are assumed in the benchmark. They offer a transparent center-spread, description and keep alpha-cut propagation straightforward. Other shapes such as trapezoidal or asymmetric fuzzy numbers may also be used when better prior information is available; that extension is left for future work.

The α-level box is therefore:

$$\mathcal{P}^{\alpha} = [\widetilde{\beta}]^{\alpha} \times [\widetilde{\mu}]^{\alpha} \times [\widetilde{\gamma}_s]^{\alpha} \times [\widetilde{\delta}]^{\alpha} \times [\widetilde{\sigma}]^{\alpha} \times [\widetilde{a}]^{\alpha}.$$

For a response quantity R, the raw interval at level α is reconstructed by vertex evaluation,

$$[R]^{\alpha} = \left[\min_{p \in \mathcal{V}^{\alpha}} R(p),\ \max_{p \in \mathcal{V}^{\alpha}} R(p)\right],$$

where $\mathcal{V}^{\alpha}$ is the set of vertices of $\mathcal{P}^{\alpha}$. Because resonance can make the continuous response non-monotone, the vertex-based envelopes are post-processed so that fuzzy nesting is preserved:

$$\widehat{R}^{-}_{\alpha_q} = \min\left(R^{-}_{\alpha_q}, \widehat{R}^{-}_{\alpha_{q-1}}\right),$$
$$\widehat{R}^{+}_{\alpha_q} = \max\left(R^{+}_{\alpha_q}, \widehat{R}^{+}_{\alpha_{q-1}}\right).$$

This projection step ensures that wider fuzzy levels always contain the narrower ones. **Figure 2** represents the triangular membership functions used for the uncertain benchmark parameters of this study.

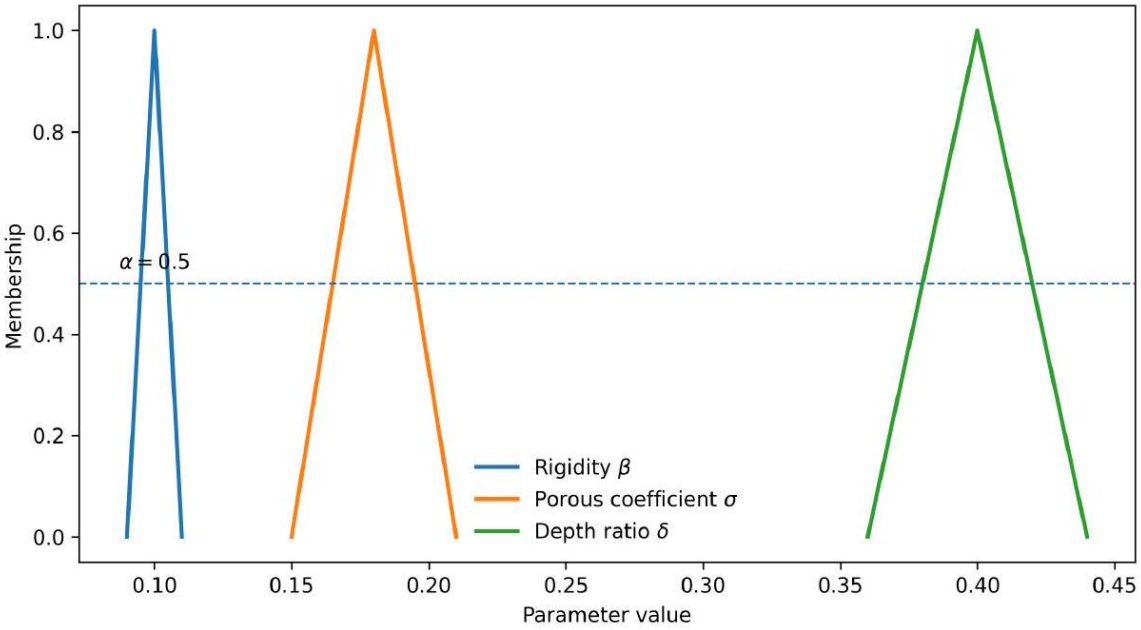

Figure 2. Representative triangular membership functions used for the uncertain benchmark parameters.

The attenuation closure is introduced as an energy-normalized benchmark split. In a physical porous breakwater, the dissipated part would depend on permeability, drag, inertial resistance, and frequency-dependent flow losses through and around the porous appendage. The present coefficient should therefore be interpreted as an effective dissipation descriptor for reduced-order analysis rather than as a fully calibrated porous-flow law[30].

2.7. Response Measures and Attenuation Closure

The main structural response quantities are the maximum deflection and the maximum bending moment,

$$|W|_{\max} = \max_{x \in [0,1]} |W(x)|,$$

$$M(x) = -\beta W''(x),\ |M|_{\max} = \max_{x \in [0,1]} |M(x)|.$$

A first-mode participation indicator is defined by:

$$q_1(\Omega) = 2\int_0^1 W(x;\Omega)\sin(\pi x)dx.$$

The wave attenuation measures are represented through the following energy-normalized closure,

$$K_t(\Omega) = \frac{1}{\sqrt{1+\alpha_r|q_1(\Omega)|^2+\alpha_p\sigma}},$$

$$K_r(\Omega) = \frac{\sqrt{\alpha_r}|q_1(\Omega)|}{\sqrt{1+\alpha_r|q_1(\Omega)|^2+\alpha_p\sigma}},$$

$$K_d(\Omega) = 1 - K_t^2(\Omega) - K_r^2(\Omega) = \frac{\alpha_p\sigma}{1+\alpha_r|q_1(\Omega)|^2+\alpha_p\sigma}.$$

The benchmark uses α_r = 0.24 and α_p = 0.65, so the three coefficients form a normalized split of the incoming wave energy into transmission, reflection, and porous loss.

2.8. Benchmark Parameters

This numerical study is built around a representative dimensionless benchmark selected to show one dominant hydro-elastic resonance together with a clear concept. The baseline parameters are listed in **Table 1** below, and the triangular fuzzy numbers are listed in the **Table 2**.

Figure 3 shows the workflow of the fuzzy Legendre-Green function under the computation model of this study.

Table 1. Baseline non-dimensional parameters of the benchmark.

Symbol	Value	Description
β	0.10	normalized flexural rigidity
μ	1.00	normalized structural mass
γ_s	0.030	structural damping
δ	0.40	depth-to-length ratio
σ	0.18	porous dissipation coefficient
a	1.00	forcing amplitude
χ_0	0.15	kernel amplitude constant
α_r	0.24	reflection closure coefficient
α_p	0.65	porous-loss closure coefficient
Ω range	2.2–3.8	frequency sweep interval
N_{ref}	160	reference collocation order

Table 2. Triangular fuzzy numbers used in the benchmark.

Parameter	Triangular Fuzzy Number
$\widetilde{\beta}$	(0.09, 0.10, 0.11)
$\widetilde{\mu}$	(0.95, 1.00, 1.05)
$\widetilde{\gamma}_s$	(0.027, 0.030, 0.033)
$\widetilde{\delta}$	(0.36, 0.40, 0.44)
$\widetilde{\sigma}$	(0.15, 0.18, 0.21)
$\widetilde{a}$	(0.90, 1.00, 1.10)

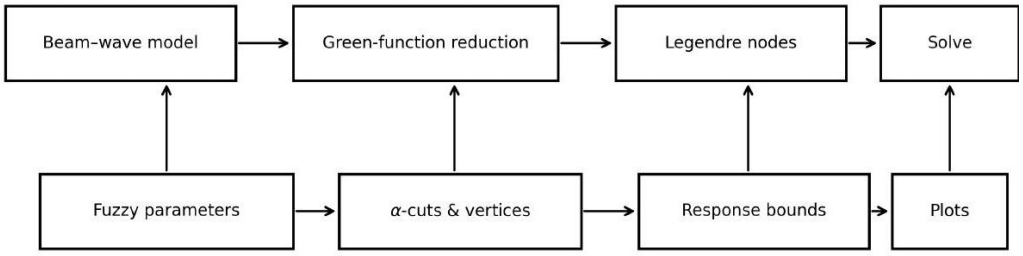

Figure 3. Computational workflow of the fuzzy Legendre-Green function method.

3. Results

3.1. Deterministic Convergence of the Solver

To address numerical robustness beyond a single point, additional trial computations across the frequency sweep showed the same stable trend: the collocation solution remained smooth away from resonance and the practical errors decreased monotonically as the order increased. The sharpest demands were observed only in the narrow resonance neighborhood, where finer discretization is naturally more valuable.

The preliminary numerical test examines and approves the deterministic benchmark at the resonance-focused frequency under this study. A high-resolution solution obtained with $N = 160$ Legendre-Gauss-Lobatto nodes is used as the numerical reference in this type of study. For any chosen discretization order N, the practical maximum-norm amplitude error is defined as follows:

$$e_\infty = \| \, |W_N| - |W_{\text{ref}}| \, \|_{L_\infty(0,1)}.$$

The observed convergence rate between two successive discretizations is estimated by:

$$p = \frac{\log\left(e_N / e_{2N}\right)}{\log 2}.$$

The resonance-focused frequency of the deterministic benchmark is given below:

$$\Omega^* = 3.125$$

(Ω^* denotes the nondimensional frequency at resonance)

At the given frequency, the response remains smooth, but the peak is sharp enough to provide a useful test for the collocation method, the convergence of the observed p is represented in **Table 3** below.

The convergence results are smooth and stable and even a modest collocation size already reproduces the main response measures with good accuracy, and the finer grids mainly confirm that the solution has settled. This is helpful for practical use, because it shows that the method does not require an unnecessarily large discretization to obtain reliable benchmark values.

Table 3. Convergence of the deterministic benchmark at Ω^*.

N	$\lvert W\rvert_{\max}$	$\lvert q_1\rvert$	K_t	e_∞	**Observed** p
10	2.213352	2.213363	0.660422	4.412×10^{-5}	-
20	2.213328	2.213338	0.660425	2.030×10^{-5}	1.12
40	2.213313	2.213323	0.660428	5.400×10^{-6}	1.91
80	2.213309	2.213319	0.660428	1.115×10^{-6}	2.28

3.2. Representative Hand Calculation at Ω = 2.80

A brief mathematical calculation is included to show the main steps of the reduced related formulation.

For $\Omega = 2.80$ and $\delta = 0.40$, the dispersion relation:

$$\Omega^2 = \kappa \tanh(\delta\kappa),$$

gives:

$$\kappa = 7.86899.$$

The porous damping contribution is then:

$$\gamma_p = \frac{\sigma\Omega}{1 + \delta\kappa} = \frac{0.18 \times 2.80}{1 + 0.40 \times 7.86899} = 0.12152,$$

so the total damping becomes

$$\gamma = \gamma_s + \gamma_p = 0.03000 + 0.12152 = 0.15152.$$

The kernel amplitude and decay rate are:

$$\chi_h = \frac{0.15 \times 2.80^2}{1 + 0.40 \times 7.86899} = 0.28354,$$
$$\eta = 0.45 + 0.25 \times 7.86899 = 2.41725.$$

For the same state, the first-mode hydrodynamic correction is:

The one-mode estimate is therefore useful as an interpretive tool away from the immediate resonance core, where the first flexural mode dominates. Its accuracy degrades close to the peak and would also deteriorate if higher-mode participation became important under different support or loading choices.

$$\Lambda_1(2.80, 0.40) \approx 0.06116.$$

Therefore,

$$D_1 = 0.10\pi^4 - 2.80^2 - i(2.80)(0.15152) + 0.06116 \approx 1.96206 - 0.42425i,$$

which implies:

$$|A_1| = \frac{1}{|D_1|} = 0.49816.$$

The full collocation solution gives:

$$|q_1| = 0.50566,\ |W|_{\max} = 0.50566,\ |M|_{\max} = 0.49907.$$

The attenuation coefficients become:

$$K_t = 0.92121,\ K_r = 0.22821,\ K_d = 0.09929.$$

This example is useful for two reasons: the first reason is to shows how the reduced analytical quantities are evaluated step by step, and the second is to confirms that the simple first-mode estimate remains close to the full collocation solution when the system is not extremely close to resonance. The calculation also makes the effect of porous damping easy to see in the final attenuation measures for this study.

3.3. Deterministic Frequency Response

The deterministic frequency sweep shows one dominant hydro-elastic resonance, and the largest structural response occurs at:

$$\Omega^* = 3.125,\ |W|_{\max} = 2.21331,\ |M|_{\max} = 2.18446.$$

The minimum transmission in the resonance band indicates that a larger share of the incoming energy is removed from direct passage. In the present benchmark, the dissipated portion remains modest, while reflection becomes the dominant companion mechanism near the peak response region. Thus, the flexible porous system in this parameter range attenuates chiefly through resonance-assisted reflection with a smaller effective porous-loss contribution.

At the same frequency,

$$K_t = 0.66043,\ K_r = 0.71610,\ K_d = 0.05103.$$

The strongest beam response therefore occurs at the same frequency where the transmission coefficient is relatively smallest. In the present closure, the resonance appears mainly through stronger reflection rather than through a peak in expected porous dissipation (see **Table 4 and Figure 4**).

The left panel of **Figure 5** shows the sharp hydro-elastic amplitude peak, while the right panel shows the corresponding attenuation indicators.

The deterministic trends are physically reasonable, and the transmission coefficient falls as the hydro-elastic amplitude grows, reaches a minimum in the resonance region, and then rises again. Reflection behaves oppositely, however, dissipation changes more gently because it is governed partly by the fixed porous coefficient and only indirectly by the resonant structural amplification.

Table 4. Deterministic response metrics at selected frequencies.

Ω	κ	γ	$\lvert q_1\rvert$	$\lvert W\rvert_{\max}$	$\lvert M\rvert_{\max}$	K_t	K_r	K_d
2.400	5.86647	0.15909	0.247044	0.247039	0.243822	0.940036	0.113769	0.103389
2.800	7.86899	0.15152	0.505665	0.505658	0.499071	0.921212	0.228206	0.099290
3.125	9.77348	0.14458	2.213320	2.213310	2.184459	0.660428	0.716103	0.051031
3.400	11.56222	0.13880	0.536921	0.536920	0.529919	0.918170	0.241512	0.098635

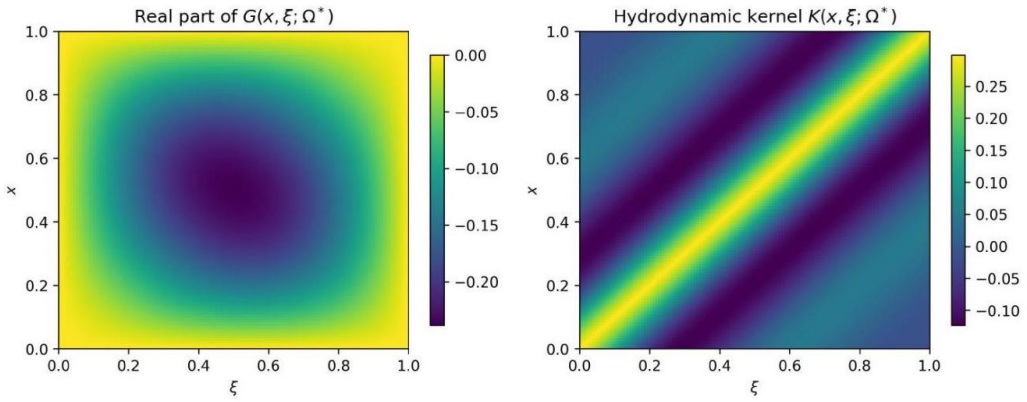

Figure 4. Deterministic Green function and reduced hydrodynamic kernel near the resonance-focused frequency.

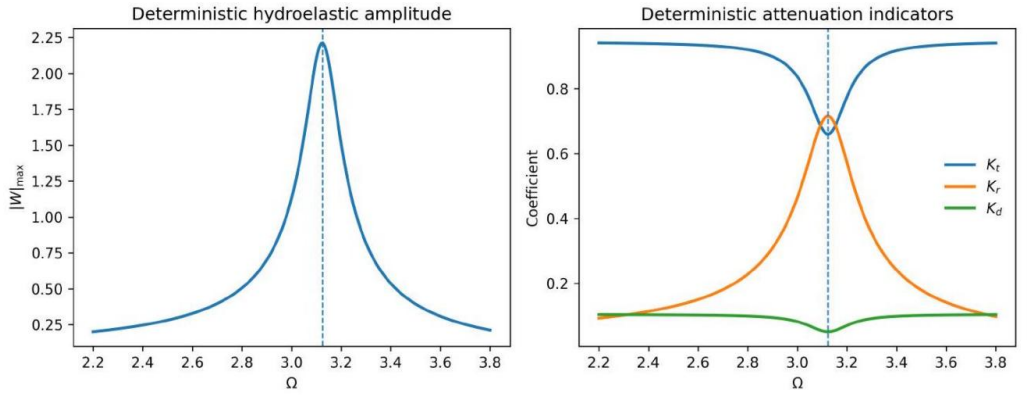

Figure 5. Deterministic structural and attenuation response over frequency.

3.4. Fuzzy Envelopes near Resonance

The fuzzy analysis is most informative close to Ω^*. At each α-level, the response is computed at all vertices of the parameter box and then projected to preserve nesting. For the maximum deflection at Ω^*,

$$\begin{aligned} [|W|_{\max}]^{\alpha=1} &= [2.213314, 2.213314] \\ [|W|_{\max}]^{\alpha=0.5} &= [1.069097, 2.232851]. \\ [|W|_{\max}]^{\alpha=0} &= [0.574875, 2.232851] \end{aligned}$$

For the transmission coefficient at the same frequency,

$$\begin{aligned} [K_t]^{\alpha=1} &= [0.660428, 0.660428] \\ [K_t]^{\alpha=0.5} &= [0.658835, 0.844833]. \\ [K_t]^{\alpha=0} &= [0.658835, 0.920119] \end{aligned}$$

These intervals show that the deterministic design point is not sufficient near resonance. Even moderate input uncertainty leads to a wide range of admissible structural amplitudes and attenuation outcomes, as shown below in **Table 5** and also visualized in **Figure 6**.

The present sensitivity study is intentionally one-at-a-time and therefore does not capture interaction effects between uncertain inputs. It is included here as a compact first diagnostic for the benchmark. A variance-based or Sobol-type global sensitivity analysis would be a natural extension once a broader uncertainty model is introduced.

The uncertainty band expands strongly near the resonance-focused frequency.

The fuzzy band is not a constant thickening of the deterministic curve. It is narrow away from resonance and wide near the minimum of the effective denominator. This is typical of resonance-controlled systems and is the main practical reason to include uncertainty in hydro-elastic breakwater assessment.

Table 5. Fuzzy intervals at the resonance-focused frequency Ω^*.

α	$\lvert W\rvert_{\max}$ Interval	Width	$\lvert M\rvert_{\max}$ Interval	Width	K_t Interval	Width
1.0	$[2.213314, 2.213314]$	0.000000	$[2.184463, 2.184463]$	0.000000	$[0.660428, 0.660428]$	0.000000
0.5	$[1.069097, 2.232851]$	1.163755	$[1.002403, 2.313933]$	1.311529	$[0.658835, 0.844833]$	0.185998
0.0	$[0.574875, 2.232851]$	1.657977	$[0.510643, 2.313933]$	1.803289	$[0.658835, 0.920119]$	0.261284

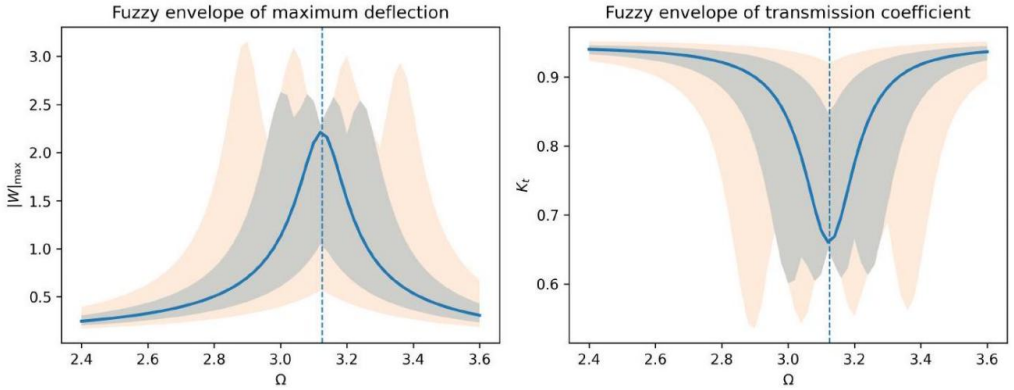

Figure 6. Fuzzy envelopes of maximum deflection and transmission coefficient in the resonance region.

3.5. Spatial Uncertainty at Resonance

The spatial distributions at Ω^* preserve the mode-like form of the deterministic solution. The widest interval of $|W(x)|$ occurs near the beam midspan, where the first flexural mode reaches its antinode. The uncertainty in the bending moment is also largest in the central region because the curvature is strongest there (see **Figure 7**).

The uncertainty width is largest near the first-mode antinode.

The pattern is consistent with the reduced mode approximation:

$$W(x) \approx A_1 \sin(\pi x),\ M(x) \approx -\beta\pi^2 A_1 \sin(\pi x).$$

Thus, the response width is geometrically concentrated near the same structural region that governs the greatest deterministic demand.

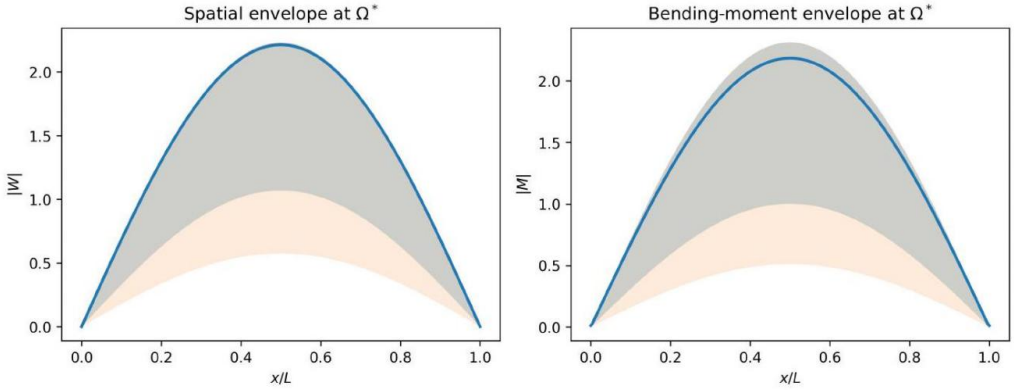

Figure 7. Spatial fuzzy envelopes of deflection and bending moment at the resonance-focused frequency.

3.6. One-at-a-Time Sensitivity

A one-at-a-time sensitivity study was performed at Ω^*. In each run, only one parameter varied across its full fuzzy support while the other five remained fixed at their deterministic values. The resulting width contributions are shown in **Table 6**.

The current methodology also faces obvious shortcomings. We thus find the hydrodynamic kernel reduced (not fully resolved), idealized support condition, effec-

tive coefficient flow term (with respect to differential permeability) instead of a full flow model with respect to permeability, and triangular fuzzy numbers with vertex evaluation in order to simplicate uncertainty computations. As such, the results should be read as benchmark-level and uncertainty-inclusive rather than a fully validated design tool. Next steps remain a stability map, direct comparison against a high-fidelity solver, and a global interaction-based sensitivity study.

This intuitively defines a fuzzy Legendre-Green function benchmark for hydro-elastic wave attenuation in a flexible porous floating breakwater. The governing beam problem was formulated as a Fredholm integral equation and was efficiently solved using Legendre-Gauss-Lobatto collocation. The numerical findings revealed a narrow resonant zone where structural response emitted strong amplifications and widening of fuzzy response envelopes. The benchmark also revealed a strong dependence of response width on porous dissipation and forcing level for the selected parameter set.

Table 6. One-at-a-time width contributions at Ω^*.

Parameter	Width Contribution to $\|W\|_{\max}$	Share (%)	Width Contribution to K_t	Share (%)
$\widetilde{\beta}$	0.004349	0.31	0.000637	0.30
$\widetilde{\mu}$	0.009165	0.65	0.001547	0.73
$\widetilde{\gamma}_s$	0.091890	6.47	0.014057	6.67
$\widetilde{\delta}$	0.277444	19.53	0.042455	20.14
$\widetilde{\sigma}$	0.595039	41.89	0.084432	40.06
$\widetilde{a}$	0.442663	31.16	0.067657	32.10

To conclude, the current formulation provides: a compact Green-function benchmark for hydro-elastic analysis; an efficient collocation-based numerical solution; a simple fuzzy uncertainty propagation framework; and physically interpretable attenuation-response trends near resonance. The model is low in computational load and scaleable, but needs to be validated against more physics faithful hydrodynamic codes on universal benchmarks before being deployed for engineering directly.

4. Discussion

At this point, the resonance peak may also be understood through the reduced maneuvering potential first-mode denominator, which plays out when its real part hovers around zero and the imaginary components are kept constrained; the amplitude quickly rises. This is characteristic of a lightly damped resonance response and accounts for why both displacement and attenuation vary rapidly over a small frequency band.

$$D_1(\Omega) = \beta\pi^4 - \Omega^2\mu - i\Omega\gamma + \Lambda_1(\Omega, \delta).$$

This same denominator also explains why, when it is large near resonance, a small change in one parameter yields no more than a mild change of the response. Because the denominator is small, that same parameter variation produces a much larger shift. Which is why uncertainty is most apparent near the "peak response" area.

This trend is also expressible in local sensitivity form, since the response magnitude is inversely dependent on the modal denominator; any perturbation that alters that denominator is amplified more strongly near resonance. The numerical results confirm this expected behavior in a very clear way.

$$A_1(\Omega) = \frac{a}{D_1(\Omega)},$$

a local perturbation gives:

$$\delta\,|A_1| \approx -\frac{|a|}{|D_1|^3}\Re\left(\overline{D_1}\delta D_1\right) + \frac{1}{|D_1|}\delta|a|.$$

If $|D_1|$is large, the same parameter change generates only a small response shift. It means that the response becomes much more sensitive if $|D_1|$ is small. These are the reasons that in this study the uncertainty band remains tight far away from resonance and widen very fast close to the resonate-driven frequency. The sensitivity ranking obtained here is benchmark-specific; however, physical sense is clear. The effective energy lost in the system is altered by porous dissipation,

whereas the response level directly gets scaled by forcing amplitude. Parameters related to stiffness and inertia are also important, but their influence is less pronounced in the selected data set.

The current results are largely consistent with the recent works on flexible floating breakwaters. Previous research indicates that flexible and dissipative components can enhance attenuation; however, hydro-elastic response may become dominant at critical operational conditions. The current model supports the same general message but adds a bounded-uncertainty view.

But one major benefit of the way we do this here, finally, is to keep things very brief yet still maintain some clear physical interpretability. The technique is therefore appropriate for early design studies and benchmarking investigations. The structural model can be extended to consider more modes, mooring effects, or nonlinear response if necessary. The hydrodynamic kernel can be replaced by a validated boundary-element or higher-fidelity interaction model. More realistic porous relations can be introduced. It would also be useful to compare fuzzy propagation with interval, stochastic, or evidence-based uncertainty models on the same benchmark.

5. Conclusions

This study presented a mathematical framework for analyzing a flexible porous floating breakwater under bounded uncertainty. The governing hydro-elastic equation was reduced with a Green function and solved by Legendre-Gauss-Lobatto collocation, which is very much addressed. Fuzzy input parameters were propagated along with alpha-cut analysis so that both structural response and wave attenuation could be examined within the same existing model. The numerical study showed a clear resonance region where response amplitudes rise sharply, and uncertainty bands widen considerably as per this study. The results discussed in this study also showed that uncertainty is concentrated near the spatial region of maximum structural response and that, for the chosen benchmark, porous dissipation and forcing level are the most influential inputs.

Finally, in this study, the method offers a practical tool for preliminary uncertainty-aware assessment of flexible porous floating breakwaters. It is mathematically and numerically transparent, computationally light, and easy to extend to many relevant situations. While it is not a replacement for a fully calibrated site-specific model but it provides a useful intermediate step between very simple reduced models and much heavier numerical simulations to address all such types of situations discussed in this study.

Author Contributions

Conceptualization, Y.N. and A.V.; methodology, Y.N.; software, Y.N. and S.I.M.; validation, A.V., M.S.S. and K.C.J.; formal analysis, Y.N. and S.I.M.; investigation, Y.N., M.S.S. and K.C.J.; resources, A.V. and M.S.S.; data curation, Y.N. and K.C.J.; writing—original draft preparation, Y.N.; writing—review and editing, A.V., M.S.S., S.I.M. and K.C.J.; visualization, Y.N. and S.I.M.; supervision, A.V. and M.S.S.; project administration, Y.N. and A.V.; funding acquisition, A.V., N.Y., and S.I.M.; All authors have read and agreed to the published version of the manuscript.

Funding

This research does not receive any external funding.

Institutional Review Board Statement

Not applicable.

Informed Consent Statement

Not applicable.

Data Availability Statement

All the data used in this study are mentioned in the manuscript itself. If any need, detailed data used in this study are available from the corresponding author upon reasonable request.

Conflicts of Interest

All authors declare there is no conflict of interest for this study.

AI Use Statement

During the preparation of this manuscript, the authors used QuillBot solely for language refinement. No AI tools were used for data analysis, interpretation, or generation of scientific content. All outputs were critically reviewed and edited by the authors. The authors take full responsibility for the integrity and accuracy of the work.

References

[1] Kara, F., 2020. Hydroelastic Behaviour and Analysis of Marine Structures. Sustainable Marine Structures. 2(1), 14–24.

[2] Amouzadrad, P., Mohapatra, S.C., Guedes Soares, C., 2024. Review of recent developments on the hydro-elastic response and gap resonance of multi-body floating structures. Ocean Engineering. 313, 119398. DOI: https://doi.org/10.1016/j.oceaneng.2024.119398

[3] Zhang, M., Schreier, S., 2022. Review of wave interaction with continuous flexible floating structures. Ocean Engineering. 264, 112404. DOI: https://doi.org/10.1016/j.oceaneng.2022.112404

[4] Ren, X., Chen, Y., Zhang, Y., et al., 2024. A discrete-module-beam hydro-elasticity method with finite element theory in analyzing VLFS in different engineering scenarios. Ocean Engineering. 307, 118121. DOI: https://doi.org/10.1016/j.oceaneng.2024.118121

[5] Pan, Z., Zhang, S., Fu, S., 2024. Integrated hydrodynamic-structural analysis of flexible floating structures. Ocean Engineering. 310(Part 1), 118644. DOI: https://doi.org/10.1016/j.oceaneng.2024.118644

[6] Jia, X., Guo, S., Wang, K., et al., 2026. Wave Attenuation Performance of a Floating Breakwater Integrated with Flexible Wave-Dissipating Structures. Journal of Marine Science and Engineering. 14(1), 97. DOI: https://doi.org/10.3390/jmse14010097

[7] Mohapatra, S., Guedes Soares, C., 2021. Hydroelastic behaviour of a submerged horizontal flexible porous structure in three-dimensions. Journal of Fluids and Structures. 104, 103319. DOI: https://doi.org/10.1016/j.jfluidstructs.2021.103319

[8] Mohapatra, S.C., Guedes Soares, C., 2022. 3D hydroelastic modelling of fluid–structure interactions of porous flexible structures. Journal of Fluids and Structures. 112, 103588. DOI: https://doi.org/10.1016/j.jfluidstructs.2022.103588

[9] Sharma, P., Sarkar, B., De, S., 2024. Oblique wave scattering by single and double inverse T-type breakwaters. Ocean Engineering. 303, 117804. DOI: https://doi.org/10.1016/j.oceaneng.2024.117804

[10] Koley, S., Mondal, R., Sahoo, T., 2018. Fredholm integral equation technique for hydroelastic analysis of a floating flexible porous plate. European Journal of Mechanics—B/Fluids. 67, 291–305. DOI: https://doi.org/10.1016/j.euromechflu.2017.10.004

[11] Yogeesh, N., Girija, D.K., Rashmi, M., 2024. Mathematical modelling techniques and applications of wireless communication using fuzzy logic. In: Mukherjee, G., Basu Mallik, B., Kar, R., et al. (Eds.). Advances on Mathematical Modeling and Optimization with Its Applications. CRC Press: Boca Raton, FL, USA.

[12] Yogeesh, N., 2024. Solving fuzzy nonlinear optimization problems using evolutionary algorithms. In: Mukherjee, G., Basu Mallik, B., Kar, R., et al. (Eds.). Advances on Mathematical Modeling and Optimization with Its Applications. CRC Press: Boca Raton, FL, USA.

[13] Rahmatov, J.S., 2025. Fuzzy differential equations: application for analyzing and predicting cyberattacks. Journal of Applied Data Analysis and Modern Stochastic Modelling. 2(2), 53–58. DOI: https://doi.org/10.64837/jadamsm.2-2-2

[14] Odinaev, R.N., 2025. Investigation of the solution of the integro-differential problem of plant protection by numerical method and an algorithm for determining unknown parameters. Journal of Applied Data Analysis and Modern Stochastic Modelling. 2(1), 30–37. DOI: https://doi.org/10.64837/JADAMSM.2-1-4

[15] Gliklikh, Y., 2025. A stochastic algebraic-differential equation of Brownian motion type with mean derivative. Journal of Applied Data Analysis and Modern Stochastic Modelling. 2(1), 1–5. DOI: https://doi.org/10.64837/JADAMSM.2-1-1

[16] Kabilov, M.M., Gulboev, B.J., 2024. Similarity of temperature and concentration fields in filtration combustion of gases. Journal of Applied Data Analysis and Modern Stochastic Modelling. 1(1), 29–38. DOI: https://doi.org/10.64837/JADAMSM.1-1-3

[17] Hemanth, S., Karmakar, D., 2025. Hydro-elastic analysis of VLFS integrated with porous floating box breakwater using multi-domain boundary element method. Marine Structures. 101, 103747. DOI: https://doi.org/10.1016/j.marstruc.2024.103747

[18] Hu, K.-Z., Xu, T.-J., Wang, S., 2025. Hydrodynamic investigation of a new type of floating breakwaters integrated with porous baffles. Applied Ocean Research. 154, 104380. DOI: https://doi.org/10.1016/j.apor.2024.104380

[19] Wang, Y.Z., Ji, C.Y., Xu, S., et al., 2025. Theoretical Study on the Wave Attenuation Performance of Floating Breakwater with a Rectangular Cross-Section. China Ocean Engineering. 39, 244–255. DOI: https://doi.org/10.1007/s13344-025-0034-5

[20] Ji, C., Lu, L., Wang, Y., et al., 2025. A New Approach for Long Wave Attenuation of Floating Breakwater: Mechanism and Validation. Engineering. In Press. DOI: https://doi.org/10.1016/j.eng.2025.09.004

[21] Hu, Y., Cheng, Y., Dai, S., et al., 2026. Hydro-elastic performance of a flexible pontoon-type floating breakwater embedded with multiple oscillating-water-column devices. Renewable Energy. 259, 125065. DOI: https://doi.org/10.1016/j.renene.2025.125065

[22] Li, S., Wei, F., Xu, H., et al., 2024. Experiment study on wave attenuation performance of a new type of porous floating breakwater. Ocean Engineering. 309(Part 2), 118334. DOI: https://doi.org/10.1016/j.oceaneng.2024.118334

[23] Amouzadrad, P., Mohapatra, S.C., Guedes Soares, C., 2025. Review on Sensitivity and Uncertainty Analysis of Hydrodynamic and Hydro-elastic Responses of Floating Offshore Structures. Journal of Marine Science and Engineering. 13(6), 1015. DOI: https://doi.org/10.3390/jmse13061015

[24] Loe, P.Y.A., Kim, M., Jin, C., et al., 2025. Recent advances in discrete-module-beam-based hydroelasticity method as an efficient tool approach for continuous very large floating structures. Ocean Engineering. 340, 122229. DOI: https://doi.org/10.1016/j.oceaneng.2025.122229

[25] Taylor, R.E., Ohkusu, M., 2000. Green functions for hydro-elastic analysis of vibrating free-free beams and plates. Applied Ocean Research. 22(5), 295–314. DOI: https://doi.org/10.1016/S0141-1187(00)00018-3

[26] Wang, L., Xiong, C., Shi, Q., 2020. An adaptive collocation method for structural fuzzy uncertainty analysis. Engineering Computations. 37(9), 2983–2998. DOI: https://doi.org/10.1108/EC-10-2018-0464

[27] Rao, S.S., Berke, L., 1997. Analysis of uncertain structural systems using interval analysis. AIAA Journal. 35(4), 727–735. DOI: https://doi.org/10.2514/2.164

[28] Zadeh, L.A., 1965. Fuzzy Sets. Information and Control. 8(3), 338–353. DOI: https://doi.org/10.1016/S0019-9958(65)90241-X

[29] Hanss, M., 2005. Applied Fuzzy Arithmetic: An Introduction with Engineering Applications. Springer: Berlin/Heidelberg, Germany. DOI: https://doi.org/10.1007/b138914

[30] Mohammad, S., Nijalingappa, Y., Karthik, M., et al., 2025. Sustainable Marine Operations: Uncertainty-Aware Multi-Body Motion Analysis of Offshore Support Vessels. Sustainable Marine Structures. 7(4), 255–275.

[31] Shekhawat, G., Livingstone, S., 2023. AI and Children's Rights: A Guide to the Transnational Guidance. Available from: https://bit.ly/3OhTG64

[32] Housley, W., Edwards, A., Beneito-Montagut, R., et al., 2023. The SAGE Handbook of Digital Society. SAGE Publications Ltd: London, UK. DOI: https://doi.org/10.4135/9781529783193